# UNIVERSITY OF BIRMINGHAM

# Effect of surface roughness and temperature on stainless steel - whey protein interfacial interactions under pasteurisation conditions

Avila-Sierra, Alejandro; Zhang, Jason; Fryer, Peter

[Link to publication on Research at Birmingham portal](#)

2      **Title**

3      **Effect of surface roughness and temperature on stainless steel - whey protein interfacial**

4      **interactions under pasteurisation conditions**

5      **Authors**

6      Alejandro Ávila-Sierra, Zhenyu Jason Zhang, and Peter J. Fryer\*

7      **Address**

8      School of Chemical Engineering, University of Birmingham, Edgbaston, Birmingham B15

9      2TT, United Kingdom

10     **Corresponding authors**

11     Peter J. Fryer       *E-mail address:* p.j.fryer@bham.ac.uk

12     **Keywords**

13     Milk fouling, surface free energy, temperature, roughness, adhesion, polarity.

19

**Abstract**

The effects of the surface characteristics of 316L stainless steel (SS316L), including chemical composition before and after foulant deposition, surface roughness, and wall temperature, on both the liquid-solid and the solid-solid interfacial interactions have been investigated using contact angle measurements and atomic force microscopy respectively. Wettability of the metal surface was favoured by increased surface roughness (in the range-limited for food contact applications) and wall temperature (within the temperature range used for pasteurisation). A fine surface finish (i.e. mirror) could be an effective intervention to reduce liquid adhesion and the subsequent foulant deposition, especially under thermal treatment. The surface free energy (SFE) of SS316L and its polar and disperse components remained constant from ambient to pasteurisation temperatures ($< 80°C$). However, as fouling develops, the surface free energy evolved: upon foulant deposition, SFE decreased. An increased polarity (3.4% from 25 to 80°C) of the fouled surface could be related to the exposure the hydrophobic core of reversibly adsorbed β-Lactoglobulin toward the foulant-air interface. Both surface adhesion and Young's modulus at sub-micron spatial resolution confirmed that the packing within the foulant and molecular orientation on the foulant surface were affected by the temperature of the underlying substrate. Temperature also affected the wetting behaviour of cleaning solutions on surface foulant; as the surface temperature increased from 25°C to 75°C, the contact angle on WPC increased, suggesting an enhanced surface hydrophobicity. Overall, this work highlights the importance of surface parameters on governing the interfacial interactions that are competing for the control of the complex fouling phenomena.

## Highlights

- Surface free energy and polarity of stainless steel remains constant over the range of operational temperatures (25 ~ 80°C).
- Surface free energy decreases upon foulant deposition.
- Polarity of the model proteinaceous foulant increases as temperature increases.
- Foulant hydrophobicity increases as the wall temperature increases.
- Liquid-surface temperature difference affects the mechanical characteristics of the deposit formed.

## Graphical Abstract
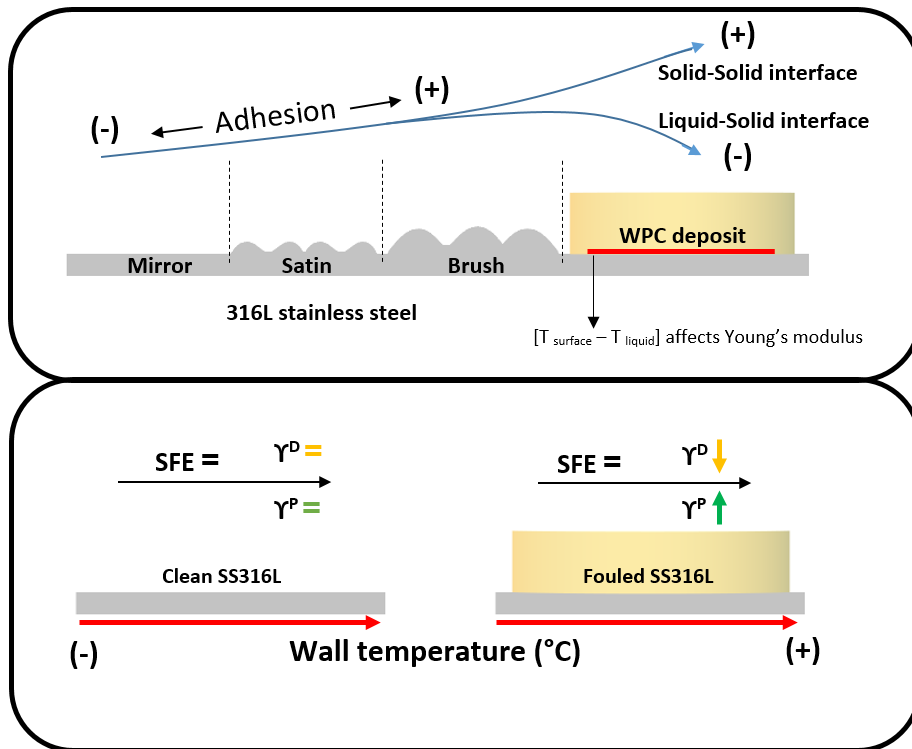
## 1. Introduction

In the dairy industry, surface fouling within pasteurisation equipment results in serious challenges for maintaining the performance of processing lines. Extensive cleaning operations are often required, which has a significant impact on the total production cost (Van Asselt et al., 2005). The cost to address issues related to heat-exchanger fouling for industrialised countries was estimated as 0.25% of the country gross national product (GNP) (Garrett-Price et al., 1985). This financial cost, alongside other issues such as product contamination, environmental impact, and industrial sustainability, emphasises the urgent need to understand fouling.

Food manufacture commonly involves equipment made of stainless steel, amongst which austenitic 304 and 316L are mostly used due to their chemical neutrality and physical durability (Schmidt et al., 2012). A range of studies have been carried out to understand and fabricate hierarchically structured surfaces, with much less attention paid to realistic engineering surfaces (Kubiak et al., 2011). The surfaces involved in a manufacturing process, including the welded joints, would be polished to meet the hygienic criteria of the installation, but even though surface roughness is well defined for food applications (Ra ≤ 0.80 μm) (Frantsen and Mathiesen, 2009), subtle variations could considerably affect interfacial interactions, especially under processing conditions.

Fouling results from interactions between the products being processed and the surfaces in contact with them, whose characteristics govern deposition and the magnitude of interfacial adhesion. At the macroscopic scale, interfacial adhesion is commonly related to surface wettability, the ability of a liquid to wet a solid surface, and contact angle measurements are used to predict the amount of foulant deposited (Handojo et al., 2009; Williams et al., 2005). The wettability of a solid substrate is determined by the balance between cohesive forces (Work

79   of cohesion: $W_c$) and adhesive forces of the liquid on a solid surface (Work of adhesion: $W_a$)

80   (Choi et al., 2002): if $W_a > W_c$, the liquid spreads over the surface, and vice versa. However,

81   surface wettability can be altered by surface characteristics such as topography (Avila-Sierra

82   et al., 2019; Zhang et al., 2015) and temperature gradients (Karapetsas et al., 2017). Kubiak et

83   al. (2011) investigated a broad spectrum of surfaces, including metallic, ceramic and polymeric

84   ones, reporting that there was a minimum contact angle below Ra < 1 μm associated with the

85   droplet spreading along the polishing grooves.

86   Contact angle measurements can be also used to quantify surface free energy (SFE), viewed as

87   a critical fouling precursor. The SFE of a given substrate offers a direct measure of the

88   intermolecular interactions at the interface (Zhao et al., 2004), and strongly influences the

89   adsorption/adhesion behaviour of compounds (such as proteins (Boxler et al., 2013;

90   Rosmaninho and Melo, 2008), cells and bacteria (Baier, 1980; Tsibouklis et al., 2000), starches

91   (Białopiotrowicz, 2003) and minerals (Boxler et al., 2013; Rosmaninho and Melo, 2008,

92   2006a)). A correlation was established between the electron-donor component of the substrate

93   and the final amount of deposit formed (Rosmaninho and Melo, 2006b), where surfaces with

94   low energy less favourable for binding (Rosmaninho and Melo, 2006b; Tsibouklis et al., 2000;

95   Zhao et al., 2007). The weaker binding at the interface, the easier the cleaning process (Akesso

96   et al., 2009). Baier et al. (1985) demonstrated the importance of both temperature and SFE on

97   bacterial adhesion at 37°C. However, very few SFE studies have studied common engineering

98   surfaces, particularly at working temperatures. Zhao et al. (2004) measured the surface free

99   energy of 304 stainless steel, alongside some other amorphous carbon surfaces, from 20 to

100  95°C, and reported that there were significant SFE variations when the testing temperature was

101  above 80°C. In addition to determining the effects that surface free energy and temperature

102  might have on surface fouling, it is critical to understand the influence that other physical (e.g.

polishing process) and chemical transformations (e.g. foulant deposition) on the metal surface might have on the interfacial interactions involved amid food processing.

During milk thermal treatment, β-Lactoglobulin (β-Lg) unfolds and exposes its hydrophobic core containing reactive disulphide and sulfhydryl bonds (Claeys et al., 2001) that can react rapidly with the processing equipment and other bulk fluid compounds (Bansal and Chen, 2006). At the nanoscale, atomic force microscopy (AFM) can determine the force/work of adhesion between a wide variety of surfaces (e.g. stainless steel, ceramic, mineral, glass and poly(tetrafluoroethylene)) (Akhtar, 2010; Navabpour et al., 2010; Sauerer et al., 2016; Verran et al., 2000) and has been used to study food confectionary foulants such as Turkish delight, caramel and sweetened condensed milk (Akhtar et al., 2010). These works highlighted differences between adhesion forces as a function of surface type, while others showed that adhesion of substrates can be measured by AFM at real process temperatures (Capella and Stark, 2006; Goode et al., 2013). When temperature increases, the work of adhesion tends to increase, especially for proteinaceous deposits that are denatured upon heating (Goode et al., 2013).

The influence of surface parameters (i.e. roughness, SFE, and temperature) on surface fouling is clear, but identifying their synergetic effects, especially under realistic conditions, will provide further insights to reduce industrial fouling. This work studies the effects of surface characteristics of 316L stainless steel on surface fouling, from nano- to macro-scale, by characterisation of surface properties before and after foulant deposition under simulated pasteurisation conditions. The objectives are (i) to determine the influence of surface characteristics on adhesion between liquid and solid (SS or foulant), (ii) to determine the extent of surface hydrophobicity as a function of surface fouling, and (iii) to establish connections between the mechanical properties of both substrates, stainless steel and foulant, and the surface parameters examined.

## 2. Materials & methods

### 2.1 Surface characterisation

Stainless steel 316L surfaces (2.54 x 2.54 cm) were prepared by using different sandpapers grit (600, 240, and 180 for mirror, satin and brush grades respectively). The process produces unidirectionally oriented substrates within the standard roughness limit defined by the 3-A Sanitary Standards (3-A SSI) and the European Hygienic Engineering & Design Group (EHEDG) for dairy industries (Ra < 0.8 µm) (Frantsen and Mathiesen, 2009). Surface roughness (Ra) was determined by White Light Interferometry (WLI) (MicroXAM2, Omniscan, U.K.) from at least four locations on each sample.

Stainless steel coupons were cleaned by the method detailed in Phinney et al., (2017): 2.0% (wt./wt.) NaOH aqueous solution at 80°C under stirring for 1 h to achieve complete removal of potential contaminants, and cooled to room temperature using a water bath. The substrates were subsequently rinsed by 1.0% (vol./vol.) HCl solution, soaked in hexane for 5 min and then acetone for another 5 min before dried by an air stream. All solvents used are HPLC grade.

### 2.2 Fouling material and procedure

A commercial whey protein concentrate (WPC) (CARBELAC 35, Carbery, Cork, Ireland) was used as received to prepare a model foulant solution (10% wt./wt.) to which the polished stainless steel coupons were exposed. Specifications of the WPC powder used are listed in **Table 1.** The model solution was prepared by mixing the WPC powder with de-ionised water at room temperature for an hour. Attention was paid to minimise aeration, foam formation, and proteins denaturation of the solution following the procedure developed in Phinney et al., (2017). To mimic relevant industrial conditions (pasteurisation temperatures, protein denaturation and surface contact time allowing ageing of the deposit), 1 ml of the prepared

151   solution was placed on the cleaned coupons (temperature kept at 25°C before deposition, unless

152   otherwise stated) and maintained at 75°C for 1 h in an oven, and then cooled. Time and

153   temperature profiles were used to minimise bubble formation, allowing gelation of the solution

154   (Phinney et al., 2017). Average fouling thickness and roughness were measured by WLI from

155   at least four different areas, and surface topography characterised using an AFM (Dimension

156   3100, Veeco, Cambridge, UK) in Tapping mode using silicon cantilevers (HQ:NSC15/AlBS

157   AFM tip; ApexProbes, UK).

158   **Table 1**. Chemical composition and protein profile of the commercial WPC powder. For chemical specification,
159   percentage is expressed by grams of component per 100 g of WPC powder. For protein profile, percentage is
160   expressed by grams of proteins per 100 g of True Protein. Data supplied by Carbery (Ballineen, Co Cork, Ireland).

161

| Chemical Specification | Total concentration (%) |
|---|---|
| Protein | 35.0 |
| Total Nitrogen | 5.5 |
| Moisture | 5.0 |
| Fat | 4.0 |
| Ash | 6.0 |
| Lactose | 50.0 |
| **Protein profile** | |
| Glycomacropeptide / Caseinomacropeptide | 27.1 |
| α -lactalbumin | 7.5 |
| Blood Serum Albumin | 4.5 |
| β-lactoglobulin | 56.7 |
| Lactoferrin | 2.0 |
| Immunoglobulin G | 2.1 |

162

## 2.3  Contact angle measurements and surface free energy characterisation

164   The sessile drop method was deployed to measure the equilibrium contact angle (ECA) for

165   wall temperatures between 25 to 80°C. ECA was quantitatively measured on a stage where the

166   influence of convective motion is negligible. A small liquid droplet was placed on the solid

167   substrate while contact angle evolution was recorded in real-time (1000 fps) by a high-speed

168   camera (FastCam SA2, Photron Europe, Bucks, United Kingdom). Stainless steel coupons

169 (with or without foulant) were placed on a heating stage monitored by a digital thermometer

170 and controlled by a thermal bath. A pipette was used to place 10 µL droplets of the testing

171 liquids on the substrate when the surface temperature is constant. ImageJ software was used

172 for image processing.

173 The set of test liquids in **Table 2** has been selected to emphasize specific molecular interactions

174 of the surfaces of interest: two non-polar liquids (diiodomethane and 1-bromonaphthalene)

175 were selected to characterise non-polar interactions, while a polar liquid (Ethylene glycol) is

176 used to model the solid surface as having two components to its surface energy, polar and non-

177 polar.

178 The **Wu method** (Wu, 1973, 1971) was selected for calculating the surface free energy (SFE)

179 of a solid substrate by dividing it into polar and disperse components. This Harmonic mean

180 model provides reliable values of both disperse and polar parts. The liquids used were 1-

181 Bromonaphthalene and ethylene glycol. The equations used for calculations are:

182 $\gamma_{sl} = \gamma_s + \gamma_l - \dfrac{4\gamma_s^d\gamma_l^d}{\gamma_s^d+\gamma_l^d} - \dfrac{4\gamma_s^p\gamma_l^p}{\gamma_s^p+\gamma_l^p}$    [1]
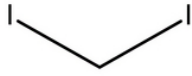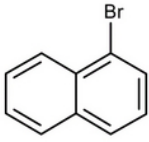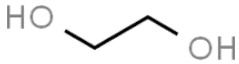
183 Combining [1] with Young's equation, the following equation can be obtained:

184 $\gamma_l(1 + \cos ECA) = \dfrac{4\gamma_s^d\gamma_l^d}{\gamma_s^d+\gamma_l^d} - \dfrac{4\gamma_s^p\gamma_l^p}{\gamma_s^p+\gamma_l^p}$    [2]

185 Where ECA is the equilibrium contact angle, $\Upsilon_{sl}$ is the interfacial tension between the solid

186 and the liquid, $\Upsilon_s$ is the overall surface energy of the solid, and $\Upsilon_l$ is the overall surface tension

187 of the wetting liquid, along with their corresponding disperse ($\Upsilon^D$) and polar components ($\Upsilon^P$).

188

**Table 2**. Properties of liquids used to characterise the equilibrium contact angle. Properties listed as a function of temperature: total surface tension of the liquid ($\Upsilon_L^T$), and corresponding disperse ($\Upsilon_L^D$) and polar components ($\Upsilon_L^P$).

| Liquid | T (°C) | Formula | $\Upsilon_L^T$ (mN/m) | $\Upsilon_L^D$ (mN/m) | $\Upsilon_L^P$ (mN/m) |
|---|---|---|---|---|---|
| Diiodomethane (Landolt and Börnstein, 1961) | 25 | | 50.0 | 50.0 | 0.0 |
| | 80 | | 42.5 | 42.5 | 0.0 |
| 1-Bromonaphthalene (Rulison, 2005) | 25 | | 44.6 | 44.6 | 0.0 |
| | 80 | | 42.2 | 42.2 | 0.0 |
| Ethylene glycol (MEGlobal, 2008) | 25 | | 47.5 | 28.7 | 18.8 |
| | 80 | | 43.6 | 26.3 | 17.3 |

## 2.4 Nano-mechanical characterisation of substrates

Nano-mechanical properties of all surfaces were quantified by atomic force microscope (AFM) (Dimension 3100, Veeco, Cambridge, UK) based force spectroscopy. A borosilicate microsphere, with a nominal diameter of 5.9 μm (Thermo Fisher Scientific, Loughborough, UK), was fixed to an AFM cantilever (ApexProbes, UK) using an epoxy adhesive (Araldite, UK) that is chemically inert. Spring constant of each cantilever was quantified using the thermal method (Hutter and Bechhoefer, 1993). Force measurements were carried out over four different locations per sample, with at least 50 force curves at each location. Adhesion force was quantified by the hysteresis upon retraction of the particle from the surface in contact. Indentation Analysis (NanoScope Analysis), using the Hertz model (spherical indenter) and fitting by the Contact Point Based method, was used to calculate Young's modulus of the substrates of interest. This method emphasises the minimum force at the contact point while minimising the influence of noise and interferences. Poisson's ratio was assumed to be 0.477 for Whey protein gels (Langley and Green, 1989) and 0.270 for SS316L surface (AZoNetwork UK Ltd, Manchester, United Kingdom).

## 2.5 Liquid cohesion and adhesion work

The work of cohesion ($W_c$) is defined as the work per unit area produced in dividing a pure liquid (**Eq. 3**), while the work of adhesion ($W_a$) is defined (**Eq. 4**) as the work required to separate two adjacent phases, in this case, a liquid-solid system (Ebnesajjad, 2006). If the ratio Wc/Wa is below one, the liquid spreads along the surface because adhesion work is larger than the cohesive one.

$$W_c = 2\gamma_L \qquad\qquad\qquad [3]$$

$$W_a = \gamma_L(1 + \mathrm{cosECA}) \qquad\qquad\qquad [4]$$

## 2.6 Statistical analysis: ANOVA

One-way analysis of variance (ANOVA) (Gelman, 2005) of both liquid contact angle and SFE of stainless steel surfaces was carried out as a function of both surface roughness and temperature to identify statistical differences between the means of two or more groups.

## 3. Results & Discussion

### 3.1 Effect of surface temperature and roughness on stainless steel wettability

Stainless steel (316L) coupons were processed to achieve three different surface finishes based on their roughness level ($R_a$): mirror ($0.03 \pm 0.01$ µm); satin ($0.31 \pm 0.01$ µm); and brush ($0.83 \pm 0.13$ µm), for which the wettability was measured as a function of both wall temperature and liquid type. Droplets of three different liquids, ethylene glycol (EG), bromonaphthalene (BN), and diiodomethane (DM), were placed on the stainless steel coupons for contact angle measurements. ECA values are summarised in **Figure 1**. It was assumed that liquid droplets completely wet the metal surface according to Wenzel (1936) (no air entrapped).

Temperature directly influences liquid properties such as surface tension, density and viscosity (Escobedo and Mansoori, 1996; Wandschneider et al., 2008). At room temperature, contact angles decreased according to liquid surface tension; DM showed the highest contact angle ($43.0 \pm 1.8°$; **Figure 1b**). At higher temperatures (25-80°C), ECAs decreased. The contact angles of EG and BN were most reduced as surface temperature increased. One-way ANOVA analysis was performed (**Table 3**), and shows significant ECA differences for EG and BN as a function of temperature. However, the wetting properties of DM did not seem to change with temperature despite its surface tension being more sensitive to the temperature than the other liquids (**Table 2**).

Surface roughness (Ra < 0.83 µm) appeared to affect the ECA measurements under the testing conditions: the rougher the surface, the greater the wetting observed. ANOVA analysis shows insignificant differences for ECA values of both EG and BN as a function of substrate roughness. However, the ECA results of DM was very responsive to roughness variations. These differences may be related to the spreading factor of those liquids (Kubiak et al., 2011).

245　Surface parameters play an important role in interfacial adhesion. Wetting of SS316L increases

246　as a function of both the surface roughness and temperature. Industrially, these results imply

247　that polishing surfaces to a high finish is effective in reducing liquid adhesion, and subsequent

248　fouling: this agrees with practice, as well as previous experimental works where significant

249　fouling reduction was observed using a mirror-finish surface instead of an unpolished one

250　(Zouaghi et al., 2018).

251

**Figure 1.** Equilibrium contact angle (ECA) as a function of both SS316L roughness and temperature. Three classes of surface finish have been used: mirror, satin, and brush. The mean values of liquid contact angles of at least three different drops per liquid are showed along standard deviation. The liquid used are 1-bromonaphthalene (a), diiodomethane (b) and ethylene glycol (c). Lines show linear regression fit to facilitate data visualisation.
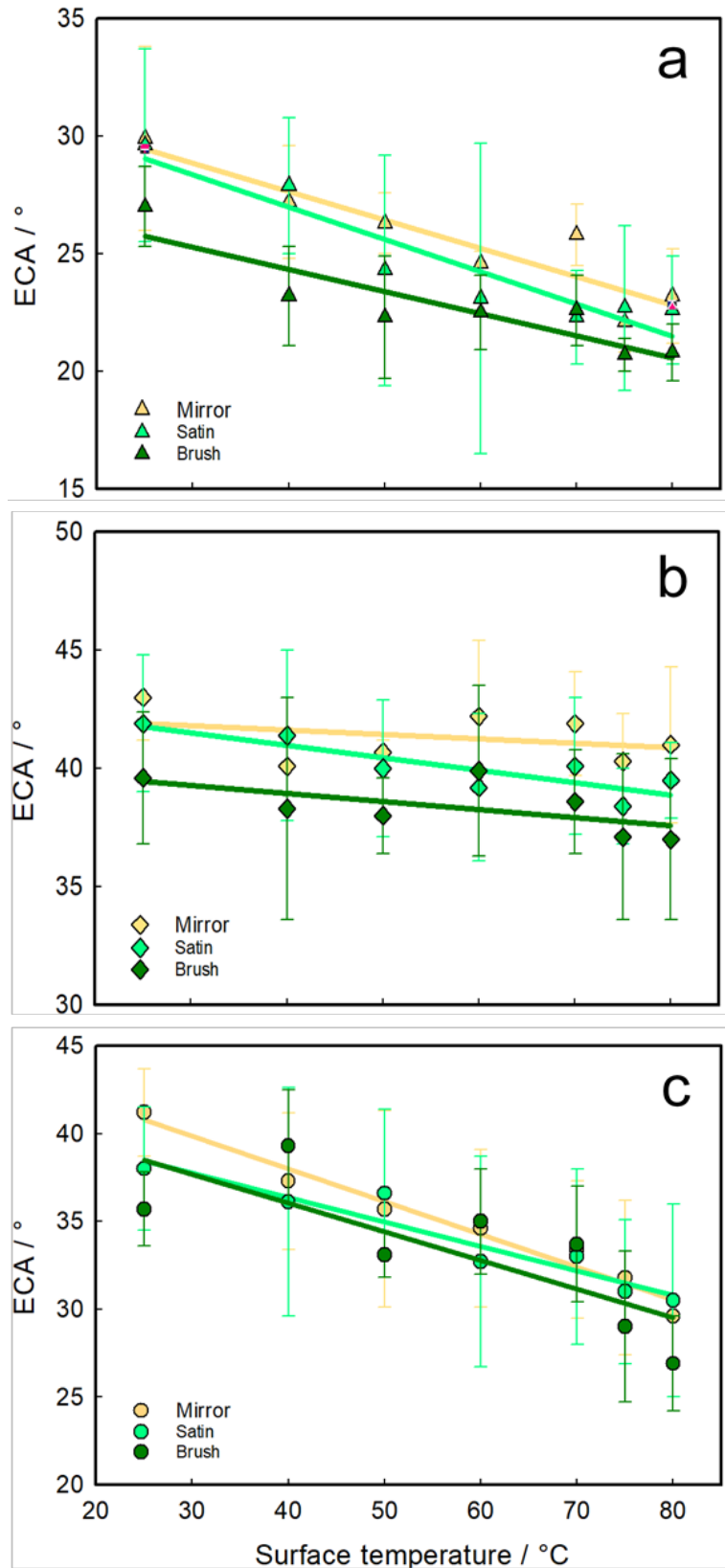
**Table 3**. One-way ANOVA analysis of both Equilibrium Contact Angle (ECA) and Surface Free Energy (SFE) measurements of clean and fouled 316L stainless steel as a function of surface temperature and roughness. F-value and p-value refer to the ratio of the variance of the group means to pooled within group variance and the probability of obtaining an F-value, respectively. P-value must be <0.05 to show a statistical significant difference between groups for the studied conditions.

| | Temperature dependence | | Roughness dependence | |
|---|---|---|---|---|
| | *F-Value* | *p-Value* | *F-Value* | *p- Value* |
| **ECA upon SS316L** | | | | |
| Diiodomethane | 1.0996 | 0.4098 | 6.9074 | 0.0059 |
| 1-Bromonaphthalene | 5.7781 | 0.0033 | 2.4257 | 0.1167 |
| Ethylene glycol | 8.1499 | 0.0006 | 0.6341 | 0.5418 |
| **SFE of SS 316L** | | | | |
| Total | 0.4156 | 0.8566 | 10.1399 | 0.0011 |
| Disperse | 0.5533 | 0.7599 | 12.5021 | 0.0004 |
| Polar | 1.4503 | 0.2645 | 0.3753 | 0.6924 |
| **ECA upon foulant** | | | | |
| Diiodomethane | 0.4958 | 0.6952 | | |
| 1-Bromonaphthalene | 0.0349 | 0.9906 | | |
| Ethylene glycol | 4.8457 | 0.0330 | | |
| **SFE of WPC foulant** | | | | |
| Total | 0.0915 | 0.9627 | | |
| Disperse | 0.4989 | 0.6933 | | |
| Polar | 6.3722 | 0.0163 | | |

## 3.2 Alteration of surface wettability upon deposition of WPC foulant

### 3.2.1 Roughness of the surface foulant

Whey protein foulant was prepared on the polished stainless steel coupons, simulating a well-formed proteinaceous layer of similar characteristics to pasteuriser deposits. The areal density and averaged thickness of this model foulant were 17.67 mg/cm$^2$ (Phinney et al., 2017) and 105.8 ± 8.6 μm respectively, which is consistent with the values for averaged fouling of raw milk after eight hours of pasteurisation (12.73 ± 0.65 mg/cm$^2$ ; SS316L plate of Ra 0.46 ± 0.2 μm) found by Barish and Goddard (2013). Surface morphology of the whey protein foulant, acquired by AFM in ambient conditions, are presented in **Figure 2**. The mean foulant roughness measured by WLI is 23 ± 6 nm, 23 ± 10 nm and 22 ± 8 nm on SS substrates with mirror, satin, and brush finishes respectively, close to that measured by AFM (12.4 ± 0.8 nm

275 over a 20 × 20 μm area). A high resolution 3D scan (**Figure 2b)** shows that the clusters are of

276 sizes less than 0.3 μm, agreeing with the previous work (Jimenez et al., 2013). The consistent

277 surface roughness values of foulants suggests that the influence of the surface finish of the

278 underlying substrate is negligible for the model foulants formed. This is likely because the

279 thickness of the foulant far exceeds the magnitude of the roughness of the coupons used. As

280 such, the effect of WPC foulant roughness was neglected for contact angle measurements.

281 **Figure 2**. Representative surface morphology images of WPC foulant prepared at 75°C for 1 hour on stainless
282 steel coupons of (a) mirror (20 × 20 μm); (b) mirror (3D image 1 × 1 μm); (c) satin and (c) brush finishes.

283



284
285
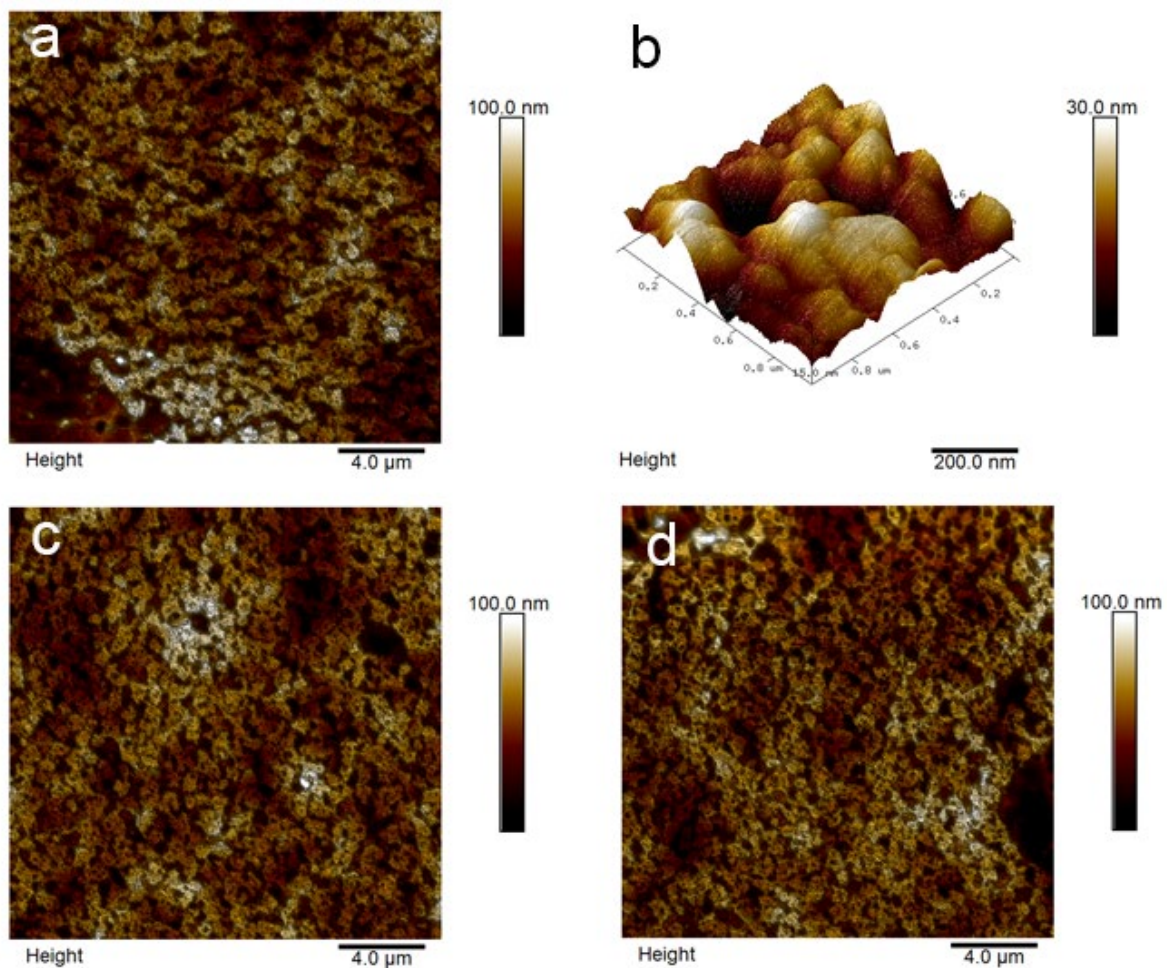
### 3.2.2 Contact angle measurements of pure liquid as a function of foulant temperature

Denaturation and aggregation reactions of β-Lactoglobulin (β-Lg) that occur at pasteurisation temperatures lead to reactions of β-Lg with processing equipment and with other bulk compounds. β-Lg adsorption and its adhesion force are favoured by increased surface temperature (Santos et al., 2003). This section aims to examine the wetting characteristics of the model foulant layer as a function of wall temperature and liquid type.

**Figure 3** presents the wettability of both stainless steel and foulant as a function of temperature for the three testing liquids, which shows temperature dependence for both substrates. The ECA of non-polar liquids remained constant as the temperature increases: DM showed greater contact angle than BN ($41.90 \pm 3.24°$ and $37.72 \pm 2.69°$ respectively) throughout the temperature range examined. While the ECA of DM was constant for both substrates, that of BN on the foulant was almost 10 degrees greater than on the bare metal surface. Although the contact angle of BN on the stainless steel coupons decreased by ca. 6° when the temperature was increased from 25 to 80°C, it remained nearly constant ($\pm 0.38°$) on the WPC deposit over the same temperature range.

The polar liquid, EG, showed the highest value at room temperature ($60.0 \pm 2.0°$), suggesting a significant reduction of surface energy at the foulant-liquid interface. When the temperature of the substrate increased, the magnitude of reduction in the ECA of EG was similar for both metal and foulant. However, the ECA of EG on stainless steel was ca. 20 degrees greater than on the formed foulant. Of the three liquids tested, EG is the only one that shows such significant statistical differences with increased temperature (**Table 3**), which suggests that changes of polar and disperse interactions could be important once foulant is formed. A proteinaceous foulant layer can alter the wettability of a substrate as a function of both liquid composition and wall temperature.

310   Surface wettability is determined by the balance between adhesive and cohesive interactions at

311   the solid-liquid interface. The ratio between the works of cohesion and adhesion of the liquids

312   tested over the mirror-finish stainless steel substrates is presented in **Table 4**.

313   For non-polar liquids, there is a reduction of the disperse forces inside the liquid drop as

314   temperature increases, promoting liquid spreading across the metal substrate. The constant

315   contact angles of the non-polar liquids on the foulant is likely due to reduction of the disperse

316   interactions, that compensate the temperature influence. For the polar liquid, increasing

317   temperature reduces the polar and disperse bonds inside the liquid, reducing cohesive

318   interactions and favouring surface wetting. It is clear that temperature has a much greater

319   influence on the ECA on the foulant than on the SS substrate, related to the increased polarity

320   at the interface.

321   Once total spreading of liquid was observed on the prepared foulant, drops of the two non-

322   polar liquids were stable at short contact times (minutes), and there was no significant

323   dissolution on the protein layer. However, the solubility of the polar liquid was favoured

324   considerably over contact time. This supports the hypothesis that polarity might be critical for

325   understanding the foulant-liquid interface.

326

**Figure 3.** Equilibrium contact angle (ECA) of the three selected liquids, 1-Bromonaphthalene, Diiodomethane, and Ethylene glycol as a function of temperature. Comparison of ECA evolution upon both substrates, (a) stainless steel and (b) WPC foulant. Error bars represent the standard error from at least three measurements.
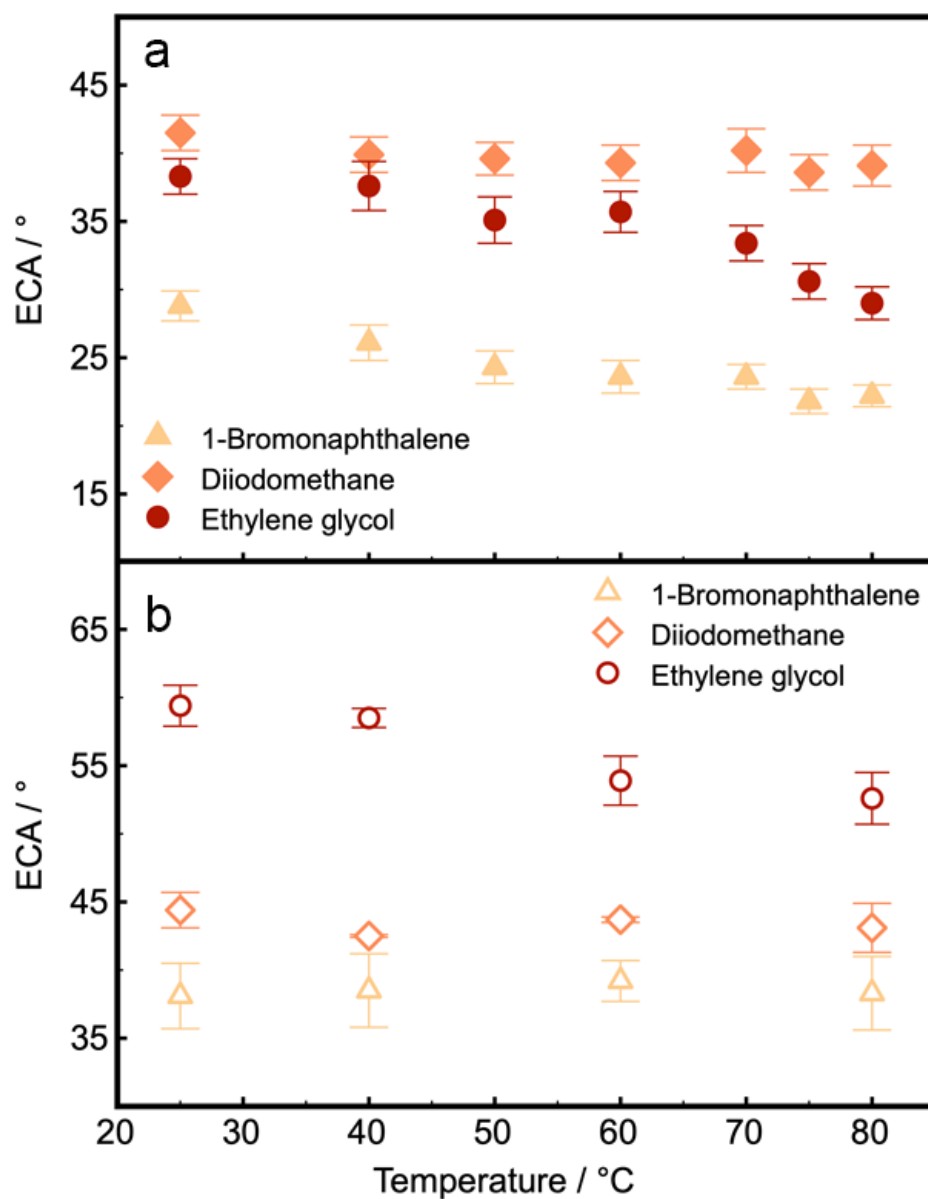
333 **Table 4**. Ratio of cohesion and adhesion work (**section 2.5**) for liquids as a function of temperature on the
334 substrates of interest (stainless steel and WPC fouling). Large ratio ($W_{cohesion}/W_{adhesion} > 1$) suggests that the liquid
335 has less tendency to spread on the substrate under the given condition, and vice versa.

336

| | | [ $W_c/W_a$ ] | | |
| --- | --- | --- | --- | --- |
| | T [°C ] | *DM* | *BN* | *EG* |
| **SS316L (mirror)** | | | | |
| | 25 | 1.16 | 1.07 | 1.14 |
| | 40 | 1.13 | 1.06 | 1.13 |
| | 50 | 1.12 | 1.06 | 1.12 |
| | 60 | 1.10 | 1.05 | 1.11 |
| | 70 | 1.08 | 1.05 | 1.10 |
| | 75 | 1.07 | 1.04 | 1.10 |
| | 80 | 1.07 | 1.04 | 1.09 |
| | *Reduction* | *0.09* | *0.03* | *0.05* |
| **WPC foulant** | | | | |
| | 25 | 1.15 | 1.12 | 1.33 |
| | 40 | 1.15 | 1.12 | 1.31 |
| | 60 | 1.15 | 1.12 | 1.27 |
| | 80 | 1.14 | 1.12 | 1.23 |
| | *Reduction* | *0.01* | *0.00* | *0.10* |

337

### 3.2.3 Contact angles of cleaning solution on WPC foulant

339 As shown in **Figures 1** and **3**, it is likely that temperature will have a significant influence on

340 the wetting behaviour of the cleaning solutions on the surface foulant, which determines the

341 removal mechanisms. **Figure 4** shows the contact angles of different cleaning formulations,

342 including water and aqueous solutions of different NaOH concentration (0.5%, 1% and 2%

343 wt./wt.), on the WPC foulant as a function of the surface temperature (25, 50 and 75°C).

344 At room temperature (25°C), water contact angle on the WPC foulant was found to be 49.0 ±

345 5.2°, slightly less than on a clean stainless steel surface (66.8 ± 9.0° for mirror and 52.4 ± 5.4°

346 for brush finishes). This is very likely due to solvation of the proteinaceous film upon contact

347 with water. As the temperature increased from 25°C to 75°C, the contact angle of water on

348 WPC increased, suggesting an enhanced surface hydrophobicity, a different characteristic to

349 that observed on bare stainless steel (**Figure 3**) where high temperature facilitated surface

350 wetting of water. Because the prepared WPC foulant consists of densely packed proteins, we

351  speculate that the adsorbed β-Lactoglobulin either exposed its hydrophobic core to the foulant-

352  air interface or denatured at increased temperature, giving increased surface hydrophobicity

353  of the WPC. Contact angles of cleaning solutions followed a similar behaviour, and according

354  to the ANOVA test in **Table 5**, there was no significant difference between ECAs of water and

355  the cleaning solutions tested. This observation highlights the critical role of molecular

356  configuration on the foulant surface in determining its wettability. Previous work suggested

357  that fast foulant removal was observed at a high temperatures (Phinney et al., 2017), which

358  confirms that cleaning is a complex process determined by not only the surface wettability of

359  the foulant, but its cohesiveness and its adhesion to the supporting substrate (stainless steel

360  here).

361  **Figure 4.** Contact angle measurements of cleaning liquids upon WPC foulant as a function of wall temperature
362  (25, 50, and 75°C). The cleaning solutions are water, NaOH 0.5%, NaOH 1%, and NaOH 2%. ANOVA analysis
363  shows non-significant differences between CAs of the cleaning solutions tested.



364
365
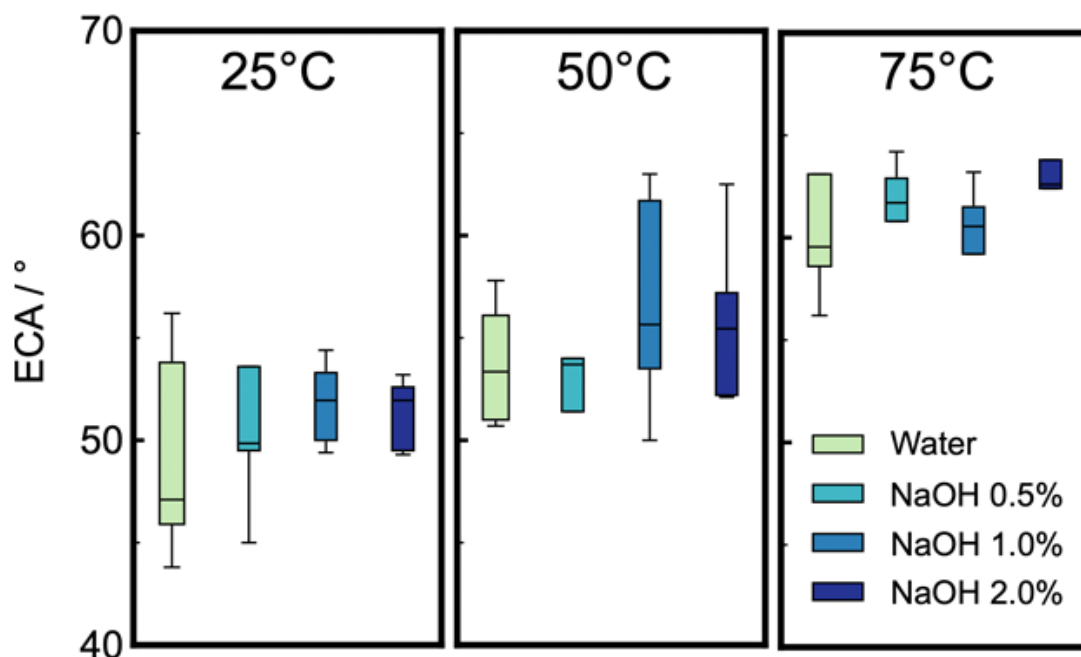
**Table 5**. One-way ANOVA analysis of the effect of both cleaning formulations and substrate temperature on the wettability of WPC fouled stainless steel 316L. F-value and p-value refer to the ratio of the variance of the group means to pooled within group variance and the probability of obtaining an F-value, respectively. P-value must be <0.05 to show a statistical significant difference between groups for the studied conditions.

| | Temperature dependence | |
| --- | --- | --- |
| | *F-Value* | *p-Value* |
| Water | 3.6823 | 0.0006 |
| NaOH 0.5% | 3.6823 | 0.0005 |
| NaOH 1% | 3.6823 | 0.0010 |
| NaOH 2% | 3.6823 | 0.0000 |

| | Effect of cleaning formulation | |
| --- | --- | --- |
| | *F-Value* | *p-Value* |
| 25°C | 3.0984 | 0.5085 |
| 50°C | 3.0984 | 0.4525 |
| 75°C | 3.0984 | 0.5069 |

370

## 3.3  Surface free energy of stainless steel and WPC foulant

**Figure 5** shows that the total surface free energy of the SS316L substrate, as well as its disperse and polar components, are independent of surface temperature ($45.4 \pm 0.6$, $39.4 \pm 0.5$, and $6.0 \pm 0.4$ mN/m respectively). The measured values of SFE are in agreement with those reported at room temperature (Barish and Goddard, 2013; Zhao et al., 2004). ANOVA analysis (**Table 3**) suggests that the polar component has no notable dependence on surface roughness and temperature, whilst the disperse component is affected by surface roughness. A previous study concerning the effects of both roughness and temperature on SFE (Avila-Sierra et al., 2019) showed that the greater surface roughness, the higher the surface energy.

Our results confirm that the SFE of stainless steel surfaces is constant in the operational window of industrial pasteurisation processes, which implies that the attractive interactions between stainless steel and the liquid being processed remain constant. SFE at room temperature could be used to estimate the free energy of the substrate under 80°C. However, other parameters such as surface roughness or alterations of liquid properties do affect the interfacial interactions.

386    The pasteurisation process, however, is more dynamic than the contact angle measurements

387    carried out in the present study – SFE of the solid substrate would evolve as the foulant

388    develops. It is therefore critical to evaluate the SFE of a model proteinaceous layer as the

389    function of temperature, upon which the underpinning formation mechanism of the foulant can

390    be established. The effect of temperature on the liquid-foulant interface is of particular interest.

391    Harmonic mean approach (**section 2.3**) was implemented to evaluate the SFE variations up to

392    80°C, with data of **Figure 5** confirming that the total SFE of the foulant remained constant

393    ($38.0 \pm 0.1$ mN/m), consistent with the observation made on stainless steel. However, the

394    dispersive and polar components of the SFE changed: there is a slight decrease of the dispersive

395    part while the polar part increases significantly, showing an increase of the foulant polarity

396    around 3.4% from 25 to 80°C (calculated as % of $\gamma_{SPolar}/\gamma_{STotal}$). ANOVA analysis (**Table 3**)

397    shows significant differences for the polar part once temperature increased. These findings

398    support our hypothesis that the adsorbed β-Lactoglobulin could adjust its molecular

399    configuration so as to expose the hydrophobic core, leading to an increased surface polarity.

400    Some previous studies confirmed the relationship between an increased amount of foulant and

401    the polar component of a wide variety of surfaces (e.g. diamond-like carbon (DLC) coatings

402    (Boxler et al., 2013), imbedded $MoS_2^{2+}$ ions, SiOx and DLC–Si–O films, Ni–P matrix with

403    PTFE particles (Rosmaninho and Melo, 2008), TiN layers (Rosmaninho et al., 2005), and

404    implantation of $SiF_3^+$ ions (Rosmaninho et al., 2007; Rosmaninho and Melo, 2006b)), where a

405    secondary protein layer could develop on the initially bound protein film through polar

406    interactions (Addesso and Lund, 1997). However, temperature not only affects fouling rate and

407    polarity of the deposit, it also affects deposit itself (Burton, 1968). As a result of increased wall

408    temperature, the increased polarity of the surface foulant might accelerate the interactions

409    between compounds at the bulk fluid and the pre-deposited material, which explains why

410    minerals tend to present in the first layer of protein deposit (Belmar-Beiny and Fryer, 1993),

411    forming a compacted structure over the processing time (Pappas and Rothwell, 1991).

412    During milk processing, the rate of heat transfer decreases with time due to the build-up of

413    surface foulant (Kukulka and Leising, 2009). Alharthi (Alharthi, 2014) identified how the

414    concentration of proteins and minerals can affect such reduction. Therefore, after the

415    development of the surface deposit, heat transfer will decrease due to the deposit

416    thickness/composition, generating a gradient of temperature inside the deposit. This implies

417    alterations of temperature that would limit the molecular interactions at the interface, and hence

418    minimise the fouling rate over time.

419    **Figure 5.** (a) Disperse, (b) Polar, and (c) Total Surface Free Energy of both SS316L (filled) and WPC foulant
420    (empty) as a function of wall temperature. Liquids tested: Ethylene glycol and 1-Bromonaphthalene. Error bars
421    represent the standard error of at least three measurements.

422



423
424
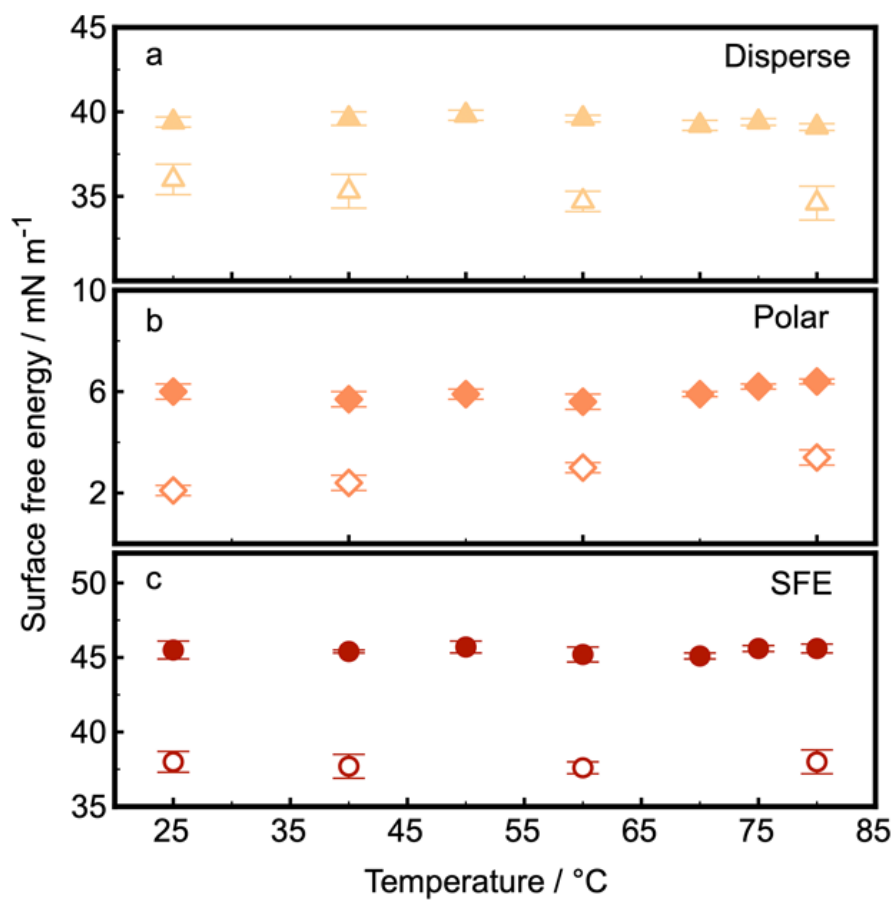
**3.4 Effect of the roughness and deposition temperature on the nanomechanical properties of the substrate**

Results suggest that the liquid-solid interface is controlled by surface parameters such as roughness and wall temperature, whilst the surface free energy data confirms that the temperature of the solid substrate influences the characteristics of the formed foulant in terms of polarity and hydrophobicity. To further decouple the effects of chemistry and roughness on the surface free energy, force spectroscopy experiments based on AFM were carried out in ambient on SS316L substrates of different finishing grades, data presented in **Figure 6a**. As demonstrated (Sauerer et al., 2016), such a technique can be effectively used as an alternative to conventional contact angle experiments with significantly improved spatial resolution. The adhesion measured between a colloidal probe (diameter ca. 6 μm) and substrate in an ambient environment is primarily determined by the capillary force that is controlled by the humidity of the environment, chemical composition, roughness, and modulus of the substrate.

For stainless steel samples, both environmental conditions and chemical composition were kept constant, and the contact area is approximately 0.056 $\mu m^2$, assuming Hertzian contact mechanics. Adhesion force on the SS substrates with mirror finish was in the range 1.5-2.5 μN, consistent with that on SS of satin finishing, but with a slightly broader distribution, as shown in **Figure 6a**. The similar range of adhesion measured on the mirror and satin samples suggests that the effect of roughness on surface energy at sub-micron scale was insignificant between those two finishes. The averaged surface adhesion increased to 3.5 μN, with a broad distribution, on the SS substrate with brush finish. Enhanced surface adhesion was likely due to the elevated contact area between the colloidal probe and the solid surface, as the result of increased surface roughness, evidenced by both the surface morphology and the scattered distribution of the adhesion force.

449　**Figure 6.** Adhesion force between an AFM colloidal probe and both (a) 316L stainless steel with mirror, satin,
450　and brush surface finishes and (b) the WPC foulant generated on 316L SS with mirror finish under controlled
451　surface temperature: 25°C, 50°C and 75°C.

452
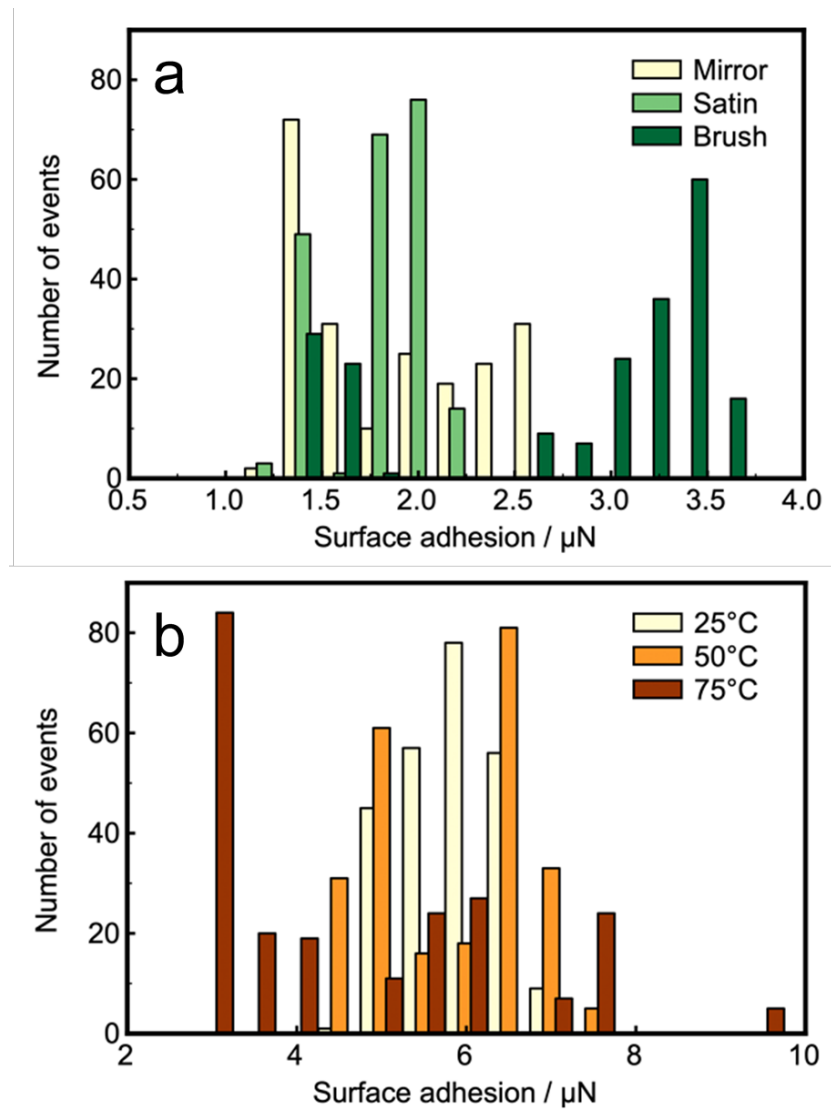


453
454

455　**Figure 6b** shows the histograms of adhesion force acquired from the proteinaceous foulant

456　developed on SS substrates of mirror finish at three different substrate temperatures. In the

457　presence of the WPC foulant, it is clear that the surface adhesion was increased to a range of

458　3-10 μN: of the several parameters that determine the surface adhesion, foulant roughness

459　probably plays only a small role, as evidenced by the morphology in **Figure 2**. The polar groups

460　on the surface of the foulant, are likely the major contributing factor for increased adhesion,

461 consistent with the contact angle results presented in **Figure 3**. Although there was only minor

462 difference between average adhesion measured on foulants formed at 25 and 50°C, there was

463 an increased range of adhesion force on the latter. This increased further on foulant prepared

464 at 75°C: adhesion force spanned a broad range, implying a heterogeneous surface, likely the

465 result of increasingly random molecular orientation.

466 The cohesiveness of the formed foulant and its correlation with the surface parameters and the

467 processing conditions, can be quantified by using AFM based nanoindentation. The Young's

468 modulus (YM) of the foulant was quantified as a function of temperature. The synergistic effect

469 of surface roughness and deformability (Young's modulus) determines the contact area

470 between two surfaces (Halvey et al., 2018; Rabinovich et al., 2000). At room temperature, there

471 is a reduction in YM from $3.9 \pm 0.7$ GPa to $3.3 \pm 1.3$ GPa for clean and fouled mirror SS

472 substrates respectively, where both materials can be viewed as hard substrates (Halvey et al.,

473 2018). For proteinaceous foulants deposited on the SS with the three different metal finishes,

474 the averaged YM remains practically constant ($3.3 \pm 1.3$ GPa and $3.2 \pm 0.4$ GPa for both fouled

475 mirror and brush metal surfaces respectively), independent of the roughness of the supporting

476 substrate. However, Young's modulus of the WPC foulant increased with temperature: $3.3 \pm$

477 $1.3$ GPa, $3.7 \pm 0.3$ GPa and $3.9 \pm 0.7$ GPa for 25, 50 and 75°C respectively, likely due to the

478 configuration of protein molecules during deposition. This again highlights the impact the first

479 foulant layer could have on the overall deposit characteristics. It is probable that the WPC

480 proteins would form a densely packed foulant layer, with less uniform molecular orientation,

481 when exposed to a mirror polish SS substrate at high temperature (75°C), whilst they would

482 construct a less densely packed and more homogeneous surface film at 25°C.

483

484

485 **4. Conclusions**

486 This work demonstrates that surface roughness, temperature, changes in surface composition,
487 as well as the temperature difference between liquid and substrate govern the interfacial
488 interactions in fouling, and therefore will control initial and subsequent formation of surface
489 layers. Wettability of 316L stainless steel is favoured by increased surface roughness and wall
490 temperature, showing how fine surface finishes are effective in reducing fouling. The surface
491 free energy (SFE) of SS316L and its components remain constant between ambient and
492 pasteurisation temperatures. However, as fouling develops, the SFE evolves. Upon foulant
493 deposition, SFE decreases, and there was a polarity increase (3.4% from 25 to 80°C) of the
494 fouled surface that might relate to the opening of the hydrophobic core of β-Lactoglobulin
495 toward the foulant-air interface. Both surface adhesion and Young's modulus at sub-micron
496 spatial resolution confirm that the molecular packing within the foulant and the molecular
497 orientation on the foulant surface are affected by the temperature of the underlying substrate,
498 showing how temperature variations in an industrial heat exchanger can result in different
499 surface deposits.

500

501

## References

502 **References**

503 Addesso, A., Lund, D.B., 1997. Influence of soild surface energy on protein adsorption. J. Food Process. Preserv.

504       21, 319–333. https://doi.org/10.1111/j.1745-4549.1997.tb00786.x

505 Akesso, L., Pettitt, M.E., Callow, J.A., Callow, M.E., Stallard, J., Teer, D., Liu, C., Wang, S., Zhao, Q., D'Souza,

506       F., Willemsen, P.R., Donelly, G.T., Kocijan, A., Jenko, M., Jones, L.A., Guinaldo, P.C., 2009. The potential

507       of nano-structured silicon oxide type coatings deposited by PACVD for control of aquatic biofouling.

508       Biofouling 25, 55–67. https://doi.org/10.1080/08927010802444275

509 Akhtar, N., Bowen, J., Asteriadou, K., Robbins, P.T., Zhang, Z., Fryer, P.J., 2010. Matching the nano- to the

510       meso-scale: Measuring deposit–surface interactions with atomic force microscopy and micromanipulation.

511       Food Bioprod. Process. 88, 341–348. https://doi.org/10.1016/j.fbp.2010.08.006

512 Akhtar, N.R., 2010. The fundamental interactions between deposits and surfaces at nanoscale using atomic force

513       microscopy. PhD thesis, University of Birmingham.

514 Alharthi, M., 2014. Fouling and cleaning studies of protein fouling at pasteurisation temperatures. PhD thesis,

515       University of Birmingham.

516 Avila-Sierra, A., Zhang, Z.J., Fryer, P.J., 2019. Effect of surface characteristics on cleaning performance for CIP

517       system in food processing. Energy Procedia 161, 115–122. https://doi.org/10.1016/j.egypro.2019.02.067

518 Baier, R.E., 1980. Substrata influences on the adhesion of microorganisms and their resultant new surface

519       properties. G. Bitton, K.S. Marshall (Eds.), Adsorption of Microorganisms to Surfaces, Wiley-Interscience

520       Publishers, New York, 59–104.

521 Baier, R.E., Depalma, V.A., Goupil, D.W., Cohen, E., 1985. Human platelet spreading on substrata of known

522       surface chemistry. J. Biomed. Mater. Res. 19, 1157–1167. https://doi.org/10.1002/jbm.820190922

523 Bansal, B., Chen, X.D., 2006. A Critical Review of Milk Fouling in Heat Exchangers. Comprehensive reviews in

524       food science and food safety. 5, 27–33. https://doi.org/10.1111/j.1541-4337.2006.tb00080.x

525 Barish, J.A., Goddard, J.M., 2013. Anti-fouling surface modified stainless steel for food processing. Food

526       Bioprod. Process. 91, 352–361. https://doi.org/10.1016/j.fbp.2013.01.003

527 Belmar-Beiny, M.T., Fryer, P.J., 1993. Preliminary stages of fouling from whey protein solutions. J. Dairy Res.

528    6, 467–483. https://doi.org/10.1017/S0022029900027837

529    Białopiotrowicz, T., 2003. Wettability of starch gel films. Food Hydrocoll. 17, 141–147.
530    https://doi.org/10.1016/S0268-005X(02)00046-2

531    Boxler, C., W., A., Scholl, S., 2013. Fouling of milk components on DLC coated surfaces at pasteurization and
532    UHT temperatures. Food Bioprod. Process. 91, 336–347. https://doi.org/10.1016/j.fbp.2012.11.012

533    Burton, H., 1968. Reviews of the progress of dairy science. J. Dairy Res. 35, 317–330.
534    https://doi.org/10.1017/S0022029900019038

535    Capella, B., Stark, W., 2006. Adhesion of amorphous polymers as a function of temperature probed with AFM
536    force–distance curves. J. Colloid Interface Sci. 296, 507–514. https://doi.org/10.1016/j.jcis.2005.09.043

537    Choi, W.Y., Park, H.J., Ahn, D.J., Lee, J., Lee, C.Y., 2002. Wettability of chitosan coating solution on "Fuji"
538    apple skin. J. Food Sci. 67, 2668–2672. https://doi.org/10.1111/j.1365-2621.2002.tb08796.x

539    Claeys, W.L., Ludikhuyze, L.R., Van Loey, A.M., Hendrickx, M.E., 2001. Inactivation kinetics of alkaline
540    phosphatase and lactoperoxidase, and denaturation kinetics of β-lactoglobulin in raw milk under isothermal
541    and dynamic temperature conditions. J. Dairy Res. 68, 95–107.
542    https://doi.org/10.1017/S002202990000460X

543    Ebnesajjad, S., 2006. 2 - Surface Tension and Its Measurement. Surf. Treat. Mater. Adhes. Bond. 9–28.
544    https://doi.org/10.1016/B978-081551523-4.50004-3

545    Escobedo, J., Mansoori, G.A., 1996. Surface Tension Prediction for Pure Fluids. AIChE J. 42, 1425–1433.
546    https://doi.org/10.1002/aic.690420523

547    Frantsen, E., Mathiesen, J.T., 2009. Specifying Stainless Steel Surfaces for the Brewery, Dairy and
548    Pharmaceutical Sectors, in: NACE Corrosion. p. 9573.

549    Garrett-Price, B., Smith, B., Watts, R., Knudsen, J., Marner, W., Suitor, J., 1985. Fouling of Heat Exchangers,
550    Characteristics, Costs, Prevention, Control and Removal. Noyes Publ. Park Ridge, NJ.

551    Gelman, A., 2005. Analysis of variance—why it is more important than ever. Ann. Stat. 33, 1–53.
552    https://doi.org/10.1214/009053604000001048

553    Goode, K.R., Bowen, J., Akhtar, N., Robbins, P.T., Fryer, P.J., 2013. The effect of temperature on adhesion forces

554	between surfaces and model foods containing whey protein and sugar. J. Food Eng. 118, 371–379.

555	https://doi.org/10.1016/j.jfoodeng.2013.03.016

556	Halvey, A.K., Macdonald, B., Dhyani, A., Tuteja, A., 2018. Design of surfaces for controlling hard and soft

557	fouling. Philos. Trans. A 377, 2138. https://doi.org/10.1098/rsta.2018.0266.

558	Handojo, A., Zhai, Y., Frankel, G., Pascall, M.A., 2009. Measurement of adhesion strengths between various milk

559	products on glass surfaces using contact angle measurement and atomic force microscopy. J. Food Eng. 92,

560	305–311. https://doi.org/10.1016/j.jfoodeng.2008.11.018

561	Hutter, J.L., Bechhoefer, J., 1993. Calibration of Atomic Force Microscope Tips. Rev. Sci. Instrum. 64, 1868.

562	https://doi.org/10.1063/1.1143970

563	Jimenez, M., Delaplace, G., Nuns, N., Bellayer, S., Deresmes, D., Ronse, G., Alogaili, G., Collinet-Fressancourt,

564	M., Traisnel, M., 2013. Toward the understanding of the interfacial dairy fouling deposition and growth

565	mechanisms at a stainless steel surface: A multiscale approach. J. Colloid Interface Sci. 404, 192–200.

566	https://doi.org/10.1016/j.jcis.2013.04.021

567	Karapetsas, G., Chamakos, N.T., Athanasios, O., Papathanasiou, G., 2017. Thermocapillary Droplet Actuation:

568	Effect	of	Solid	Structure	and	Wettability.	Langmuir	33,	10838–10850.

569	https://doi.org/10.1021/acs.langmuir.7b02762

570	Kubiak, K.J., Wilson, M.C.T., Mathia, T.G., Carra, S., 2011. Dynamics of contact line motion during the wetting

571	of rough surfaces and correlation with topographical surface parameters. Scanning 33, 370–377.

572	https://doi.org/10.1002/sca.20289

573	Kukulka, D.J., Leising, P., 2009. Evaluation of Surface Coatings on Heat Exchangers. Chem. Eng. Trans. 18,

574	339–344.

575	Landolt, H., Börnstein, R., 1961. Numerical Data and Functional Relationships in Science and Technology. New

576	Ser. 16, 144.

577	Langley, K.R., Green, M.L., 1989. Compression strength and fracture properties of model particulate food

578	composites in relation to their microstructure and particle-matrix interaction. J. Texture Stud. 20, 191–207.

579	https://doi.org/10.1017/S0022029900026480

580	MEGlobal, 2008. Ethylene Glycol Product Guide.

581    Navabpour, P., Teer, D., Su, X., Liu, C., Wang, S., Zhao, Q., Donik, C., Kocijan, A., Jenko, M., 2010.

582        Optimisation of the properties of siloxane coatings as anti-biofouling coatings: Comparison of PACVD and

583        hybrid PACVD–PVD coatings. Surf. Coatings Technol. 204, 3188–3195.

584        https://doi.org/10.1016/j.surfcoat.2010.03.011

585    Pappas, C.P., Rothwell, J., 1991. The effects of heating, alone or in the presence of calcium or lactose, on calcium

586        binding to milk proteins. Food Chem. 42, 183–201. https://doi.org/10.1016/0308-8146(91)90033-K

587    Phinney, D.M., Goode, K.R., Fryer, P.J., Heldman, D., Bakalis, S., 2017. Identification of residual nano-scale

588        foulant material on stainless steel using atomic force microscopy after clean in place. J. Food Eng. 214,

589        236–244. https://doi.org/10.1016/j.jfoodeng.2017.06.019

590    Rabinovich, Y., Adler, J.J., Ata, A., Singh, R.K., Moudgil, B.M., 2000. Adhesion between Nanoscale Rough

591        Surfaces. J. Colloid Interface Sci. 232, 10–16. https://doi.org/10.1006/jcis.2000.7167

592    Rosmaninho, R., Melo, L.F., 2008. Protein–calcium phosphate interactions in fouling of modified stainless-steel

593        surfaces by simulated milk. Int. Dairy J. 18, 72–80. https://doi.org/10.1016/j.idairyj.2007.06.008

594    Rosmaninho, R., Melo, L.F., 2006a. The effect of citrate on calcium phosphate deposition from simulated milk

595        ultrafiltrate (SMUF) solution. J. Food Eng. 73, 379–387. https://doi.org/10.1016/j.jfoodeng.2005.02.017

596    Rosmaninho, R., Melo, L.F., 2006b. Calcium phosphate deposition from simulated milk ultrafiltrate on different

597        stainless steel-based surfaces. Int. Dairy J. 16, 81–87. https://doi.org/10.1016/j.idairyj.2005.01.006

598    Rosmaninho, R., Rizzo, G., Muller-Steinhagen, H., Melo, L.F., 2005. Anti-fouling stainless steel based surfaces

599        for milk heating processes, in: Proceedings of 6th International Conference on Heat Exchanger Fouling and

600        Cleaning - Challenges and Opportunities.

601    Rosmaninho, R., Santos, O., Nylander, T., Paulsson, M., Beuf, M., Benezech, T., Yiantsios, S., Andritsos, N.,

602        Karabelas, A., Rizzo, G., Müller-Steinhagen, H., Melo, L.F., 2007. Modified stainless steel surfaces targeted

603        to reduce fouling – Evaluation of fouling by milk components. J. Food Eng. 80, 1176–1187.

604        https://doi.org/10.1016/j.jfoodeng.2006.09.008

605    Rulison, C., 2005. Effect of Temperature on the Surface Energy of Solids. KRUSS Application Note AN250e.

606    Santos, O., Nylander, T., Rizzo, G., Müller-Steinhagen, H., Trägårdh, C., Paulsson, M., 2003. Study of whey

607        protein adsorption under turbulent flow rate, in: Proceedings of Heat Exchanger Fouling and Cleaning—

608   fundamentals and Applications. p. 24.

609 Sauerer, B., Stukan, M., Abdallah, W., Derkani, M.H., Fedorov, M., Buiting, J., Zhang, Z.J., 2016. Quantifying

610   mineral surface energy by scanning force microscopy. J. Colloid Interface Sci. 472, 237–246.

611   https://doi.org/10.1016/j.jcis.2016.03.049

612 Schmidt, R.H., Erickson, D.J., Sims, S., Wolff, P., 2012. Characteristics of Food Contact Surface Materials:

613   Stainless Steel. Food Prot. Trends 32, 574–584.

614 Tsibouklis, J., Stone, M., Thorpe, A.A., Graham, P., Nevell, T.G., Ewen, R.J., 2000. Inhibiting bacterial adhesion

615   onto surfaces: the non-stick coating approach. Int. J. Adhes. Adhes. 20, 91–96.

616   https://doi.org/10.1016/S0143-7496(99)00034-2

617 Van Asselt, A.J., Vissers, M.M.M., Smit, F., De Jong, P., 2005. In-line control of fouling., Heat Exchanger Fouling

618   and Cleaning—Challenges and Opportunities, Engineering Conferences International Kloster Irsee,

619   Germany, 5-10 June (Engineering Conferences International, New York, USA).

620 Verran, J., Rowe, D.L., Cole, D., Boyd, R.D., 2000. The use of the atomic force microscope to visualise and

621   measure wear of food contact surfaces. Int. Biodeterior. Biodegradation 42, 99–105.

622   https://doi.org/10.1016/S0964-8305(00)00070-6

623 Wandschneider, A., Lehmann, J.K., Heintz, A., 2008. Surface Tension and Density of Pure Ionic Liquids and

624   Some Binary Mixtures with 1-Propanol and 1-Butanol. J. Chem. Eng. Data 53, 596–599.

625   https://doi.org/10.1021/je700621d

626 Wenzel, R.N., 1936. Resistence of solid surfaces to wetting by water. Ind. Eng. Chem. Res. 28, 988.

627 Williams, A.M., Jones, J.R., Paterson, A.H.J., Pearce, D.L., 2005. Milks and milk concentrates: surface tension

628   measurement. Int. J. Food Eng. 1, 1556–3758. https://doi.org/10.2202/1556-3758.1002

629 Wu, S., 1973. Polar and Nonpolar Interactions in Adhesion. J. Adhes. 5, 39–55.

630   https://doi.org/10.1080/00218467308078437

631 Wu, S., 1971. Calculation of interfacial tension in polymer systems: Polymer Symposia. J. Polym. Sci. Polym.

632   Symp. 34, 19–30. https://doi.org/10.1002/polc.5070340105

633 Zhang, P., Wang, S., Wang, S., Jiang, L., 2015. Superwetting Surfaces under Different Media: Effects of Surface

634   Topography on Wettability. Small nano micro 11, 1939–1946. https://doi.org/10.1002/smll.201401869

635 Zhao, G., Raines, A.L., Wieland, M., Schwartza, Z., Boyan, B.D., 2007. Requirement for both micron- and
636 submicron scale structure for synergistic responses of osteoblasts to substrate surface energy and
637 topography. Biomaterials 28, 2821–2829. https://doi.org/10.1016/j.biomaterials.2007.02.024

638 Zhao, Q., Liu, Y., Abel, E.W., 2004. Effect of temperature on the surface free energy of amorphous carbon films.
639 J. Colloid Interface Sci. 280, 174–183. https://doi.org/10.1016/j.jcis.2004.07.004

640 Zouaghi, S., Six, T., Nuns, N., Simon, P., Bellayer, S., Moradi, S., Hatzikiriakos, S.G., André, C., Delaplace, G.,
641 Jimenez, M., 2018. Influence of stainless steel surface properties on whey protein fouling under industrial
642 processing conditions. J. Food Eng. 228, 38–49. https://doi.org/10.1016/j.jfoodeng.2018.02.009

643